Applied Materials Today 36 (2024) 102070

Contents lists available at ScienceDirect

Applied Materials Today

journal homepage: www.elsevier.com/locate/apmt

Induction of macrophage polarization by electrospun nano-yarn containing naproxen sodium to promote tendon repair

Xiao Yu [a,1], Guiwang Shen [b,1], Jiujiu Yan [c], Wanxin Guo [a], Zhengchao Yuan [a], Jie Cui [a], Yihong Shen [a], Pengfei Cai [a], Yujie Chen [a], Mok Tsz Ngai [b,d], Mohamed EL-Newehy [e], Hany EL-Hamshary [e], Binbin Sun [a,*], Jieruo Li [b,*], Xiumei Mo [a,*]

[a] State Key Laboratory for Modification of Chemical Fibers and Polymer Materials, Shanghai Engineering Research Center of Nano-Biomaterials and Regenerative Medicine, College of Biological Science and Medical Engineering, Donghua University, 201620, Shanghai, China
[b] Department of Joint and Sport Medicine, First Affiliated Hospital of Jinan University, 613 Huangpu West Avenue, 510632, Guangzhou, Guangdong, China
[c] College of Textiles, Donghua University, 201620, Shanghai, China
[d] Department of Infectious Diseases and Public Health, Jockey Club College of Veterinary Medicine and Life Sciences, City University of Hong Kong, 000000, Hong Kong, China
[e] Department of Chemistry, College of Science, King Saud University, P.O. Box 2455, Riyadh 11451, Saudi Arabia

ARTICLE INFO

Keywords:
Electrospinning
Tendon repair
Naproxen sodium
Anti-inflammatory

ABSTRACT

Excessive inflammatory response can lead to failure of the tendon repair surgery. Tendon substitutes that can effectively balance inflammatory responses and have sufficient mechanical properties are one of the key factors in promoting repair. In this study, the nanofibers containing the naproxen sodium were attached to polylactic acid micron yarn by electrospinning to obtain double-layer core-spun yarn (DY). The DY was knitted into a tendon tissue engineering scaffold with sufficient mechanical properties. This study confirmed the optimal loading concentration of naproxen sodium. The results *in vitro* and *in vivo* indicated that sustained-release naproxen sodium in scaffolds could effectively inhibit the rapid proliferation of foreign fibroblasts, accelerate the polarization of macrophages, reduce the inflammatory response, and promote tendon tissue repair. This study provides a new scaffold for tendon tissue engineering that not only serves as a substitute for tendon repair, but also serves as an anti-inflammatory agent to better promote the repair process.

1. Introduction

Tendons are connective tissues that connect muscle to bone and are essential for joint stability and movement. However, tendon injuries or ruptures caused by overuse, trauma, and other reasons can affect people's normal lives such as severe pain, serious joint dysfunction, and even lifelong disability [1,2]. Surgery can repair the ruptured tendon, but the probability of a second surgery is high, which is often associated with complications in tendon repair [3]. Complications are related to many factors, such as the inflammatory response, foreign fibroblasts excessive proliferation, and wound infection [4,5]. Although inflammation is necessary to initiate the healing process and remove damaged tissue, excessive inflammation leads to tenocyte death, matrix degradation, and scar formation, impeding tendon recovery of tendon structure and strength [6]. Therefore, one of the keys to promoting tendon repair is to reduce the inflammatory response [7,8].

There are several techniques for tendon repair, among which electrospinning is a technique that can mimic biological fibers of extracellular matrix (ECM) [9,10]. Nanofibers have controllable fiber size and high surface-to-volume ratio to promote cell proliferation and differentiation, which are beneficial for tissue repair [11,12]. Nanofiber membranes can act as carriers of anti-inflammatory drugs used for tissue repair [13–15]. Jiang et al. [16] prepared celecoxib-loaded electrospun nanofiber membranes that could down-regulate ERK1/2 and SMAD2/3 phosphorylation, reduce inflammatory response, and inhibit fibroblast proliferation. However, when tendons require an alternative scaffold that has sufficient mechanical properties and the ability to regulate the inflammatory response, nanofiber membranes cannot meet the demand due to their poor mechanical properties [17]. Wu et al. [18] developed hybrid yarns that had better mechanical properties compared with

* Corresponding authors.
E-mail addresses: binbin.sun@dhu.edu.cn (B. Sun), ilorugaie@163.com (J. Li), xmm@dhu.edu.cn (X. Mo).
[1] Xiao Yu and Guiwang Shen contributed equally to this work

https://doi.org/10.1016/j.apmt.2024.102070
Received 4 October 2023; Received in revised form 2 January 2024; Accepted 10 January 2024
2352-9407/© 2024 Elsevier Ltd. All rights reserved.

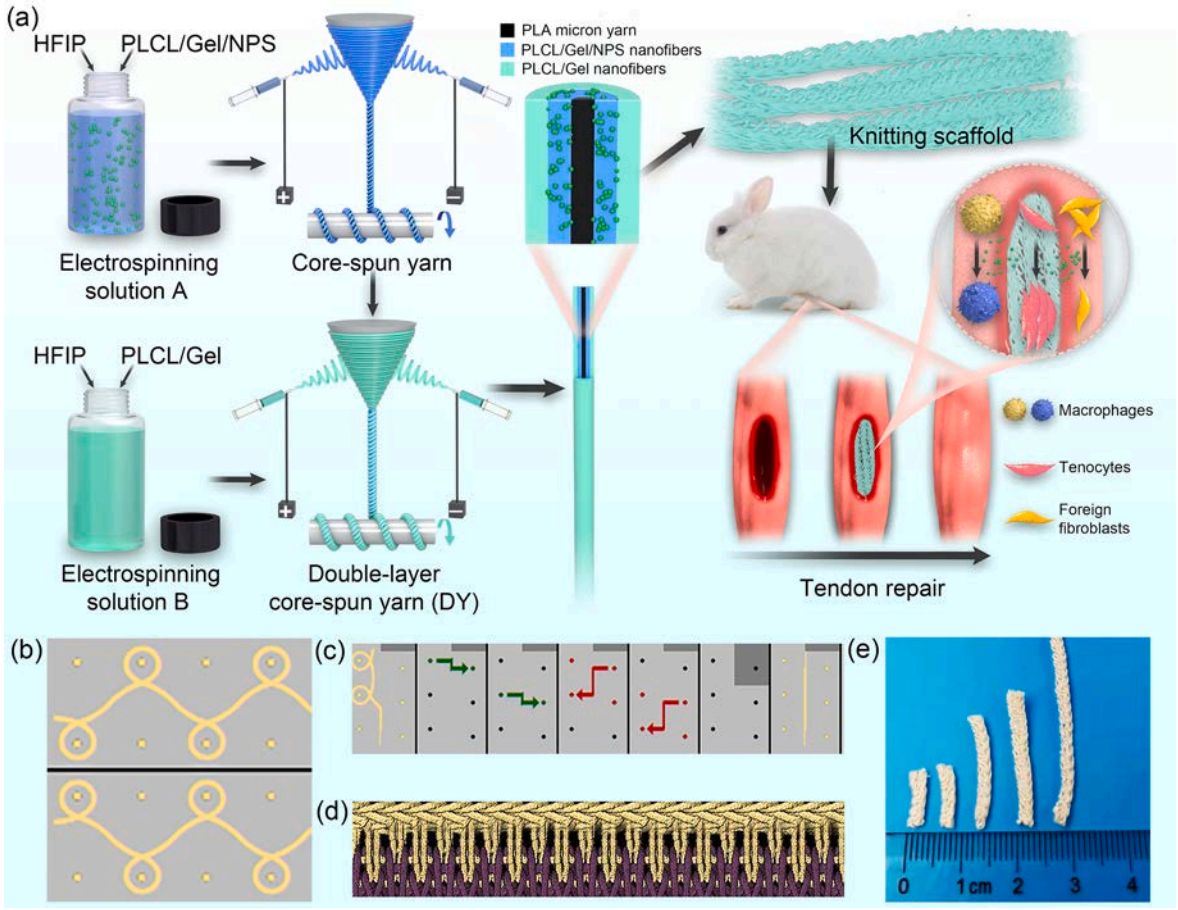

Fig. 1. Schematic illustration of the preparation of the DY (a): Firstly, the nanofibers of PLCL/Gel/NPS were wrapped around PLA micron yarn to form core-spun yarn under voltage. Secondly, the nanofibers of PLCL/Gel were wrapped around the core-spun yarn to form DY under voltage. Thirdly, three strands of DY were combined into one strand and knitted according to the program. Then, knitting scaffolds could promote tenocytes proliferation, and the NPS released from the knitting scaffolds could regulate the polarization of macrophages toward M2 and inhibit the proliferation of foreign fibroblasts. Finally, the knitting scaffolds were implanted into the defective patellar tendon of the rabbit to promote repair. DY knitting program (b). DY knitting end program (c). Computer-generated structure schematic illustration of the knitting scaffold (d). The macroscopic picture of the knitting scaffolds (e).

nanofiber membranes, which could induce cell proliferation and directional arrangement. At present, yarns are woven, knitted, and artificially woven into tendon replacement scaffolds that can mimic the mechanical properties and biological functions of natural tendons [19,20]. However, the previous scaffolds were more like knitting a piece of "cloth", which could only be applied through cutting. During the cutting process, the "cloth" was prone to loosening [21]. Therefore, it is necessary to develop a knitting scaffold with good mechanical properties, stable structure, and functionality.

The inflammation and oxidative stress are aggravated within 24 h after the tendon injury caused by acute trauma [22–24]. Reactive oxygen species (ROS) are produced in the upstream mechanism in the cyclooxygenase-2 (COX-2) pathway of the inflammatory stage, which will change the inactive binding state of NF-kB and IkB into the active state of NF-kB, and increase the expression of inflammatory cytokines such as TNF-a and IL-6 in the downstream pathway [25–27]. Thus, reduced accumulation of ROS and inflammatory cytokines in the COX-2 pathway is critical to tendon repair [28,29]. Naproxen sodium (NPS) is a non-steroidal anti-inflammatory drug with strong selective inhibition of COX-2, resulting in strong anti-inflammatory effects and few side effects [30,31]. Polylactic acid (PLA) has good biodegradability and tensile strength, low-cost, safe, and pollution-free [32]. Poly (L-lactide-co-caprolactone) (PLCL) is a biodegradable synthetic polymer with excellent mechanical properties, but PLCL is a hydrophobic material that is not conducive to cell adhesion [33]. Gelatin (Gel) is a hydrophilic material with good biocompatibility and biodegradability. It has an Arg-Gly-Asp domain, which provides recognition sites for cell adhesion [34].

In this study, a three-dimensional (3D) scaffold containing NPS was prepared by combining electrospinning and knitting technology for tendon injury repair. PLCL, Gel, and NPS were used to prepare the nanofibers by electrospinning, which were wrapped on the PLA micron yarn. The nanofibers mimicked the ECM to provide a microenvironment for cell growth. The PLA micron yarn acted as a reinforcing core to provide the mechanical properties of the scaffold. NPS could reduce the levels of pro-inflammatory cytokines and inhibit the proliferation of foreign fibroblasts, thus promoting tendon repair. During the knitting process, different knitting programs could be designed to get personalized 3D scaffolds. The clever tail-needle design could remove waste yarn in one step, thus not damaging the overall structure of the scaffold. Moreover, the scaffold could be cut freely without loosening. Therefore, the scaffold has become more ingenious, personalized, and stable by improving the knitting method.

2. Experiments and methods

2.1. Materials

The poly(L-lactide-co-caprolactone) [PLCL, LA: CL=75:25, IV (dl/g): 2.8] was purchased from Jinan Daigang Biomaterial Co., Ltd (Shandong,

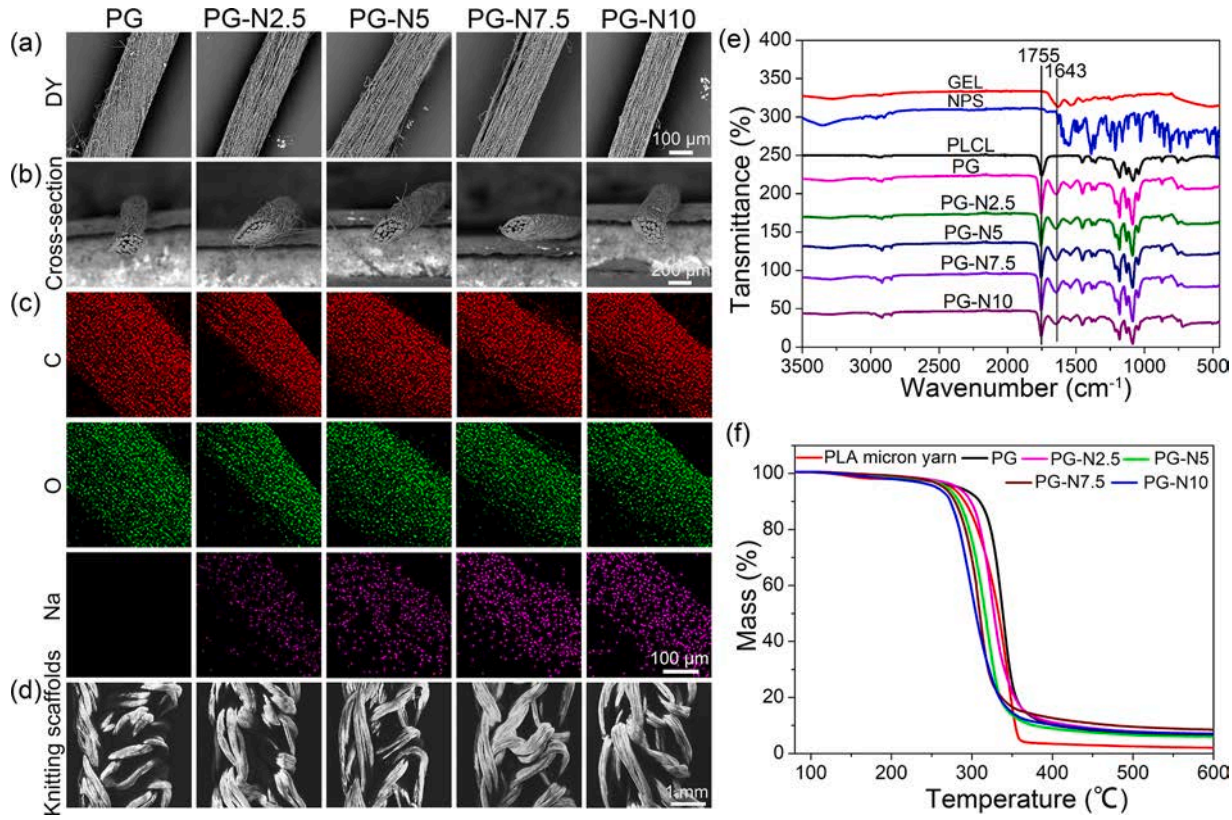

Fig. 2. SEM images of the DY (a), scale bar = 100 μm. Cross-section of DY (b), scale bar = 200 μm. EDS mapping images of DY (c), scale bar = 100 μm. SEM images of the knitting scaffolds (d), scale bar = 1 mm. FTIR spectra of the Gel, NPS, PLCL, PG, and NPS-incorporated DY (e). TGA curves of PLA micron yarn, PG, and NPS-incorporated DY (f). (n = 3).

China). Gelatin (Gel, S30952–100 G) was purchased from Shanghai Yuanye Biotechnology Co., Ltd (Shanghai, China). Naproxen sodium (NPS, 99 %, F21356–5 G) was purchased from Shanghai Merrill Chemical Technology Co., Ltd (Shanghai, China). Polylactic acid (PLA) micron yarn was purchased from Shanghai Taixin New Material Technology Co., Ltd (Shanghai, China) and 1,1,1,3,3,3-hexafluoro-2-propanol (HFIP) was purchased from Shanghai Jiu Ming Trading Firm (Shanghai, China). Rat bone marrow mesenchymal stem cells (rBMSCs) and tenocytes were extracted from two-week-old SD rats according to the previous report [16,35], and the SD rats were purchased from Shanghai JieSiJie Laboratory Animal Co., Ltd. (Shanghai, China). RAW264.7 and NIH 3T3 were obtained from the Cell Bank of the Chinese Academy of Sciences (Shanghai, China).

2.2. Preparation of DY and knitting scaffolds

Two spinning solutions were prepared, namely spinning solution A and spinning solution B. Spinning solution A: 0.7 g PLCL, 0.3 g Gel, and NPS of different quality (0 mg, 25 mg, 50 mg, 75 mg, 100 mg) were dissolved in 10 mL of HFIP solvent. Spinning solution B: 0.7 g PLCL, 0.3 g Gel dissolved in 10 mL of HFIP. The solution was stirred for 12 h at room temperature until completely dissolved. DY was fabricated by electrospinning (Fig. 1a): The PLA micron yarn passed through the winding roll and was fixedly connected to the receiving roll. Two syringes containing spinning solution A were placed at the two ends of the equipment. Under the action of voltage and winding roll, the nanofibers containing NPS as a middle layer adhered to the surface of PLA micron yarn to obtain core-spun yarn. The spinning solution B was spun on the basis of core-spun yarn, thus the outer fibers wrapped the middle layer fibers to form DY. The parameters of electrospinning were as follows: the voltage was 8.5 kV; the propulsion speed was 0.02 mL/min; the receiving speed was 10 rpm; and the winding roll speed was 400 rpm. The DY was crosslinked for 40 min in glutaraldehyde and then aired in a fume hood for 3 days to remove residual solvent.

Three strands of DY were combined into one strand by using a high-precision computerized flat knitting machine (stone TTsports, Germany), and then knitted according to the program (Fig. 1b–d). The parameters of the machine were as follows: machine speed was 0.1 m/s; needle position was 8.5. After knitting, the waste yarn was removed to obtain a complete 3D knitting scaffold. The length of the knitting scaffold could be adjusted by cutting according to the actual demand (Fig. 1e). The DY and knitting scaffold were named PG, PG-N2.5, PG-N5, PG-N7.5, and PG-N10 according to the content of NPS in each milliliter of spinning solution.

2.3. Characterization of DY and knitting scaffolds

The characterization of DY and knitting scaffolds were as follows: scanning electron microscopy (SEM), element analysis by energy dispersive spectrometer (EDS), Fourier transform infrared spectroscopy (FTIR), mechanical testing, water contact angle test, thermogravimetric analysis (TGA), *in vitro* degradation and drug release. A detailed description of the related methods is provided in the Supplementary Information.

2.4. Cytocompatibility and anti-inflammatory ability of knitting scaffolds

Different cells including rBMSCs, RAW264.7, NIH 3T3, and tenocytes were used to evaluate the biocompatibility and anti-inflammatory ability of the knitting scaffolds. The experiment includes cell extraction, cell culture, cell seeding, cytotoxicity, cell proliferation, fluorescent staining, cell adhesion, anti-oxidant and anti-inflammatory, and cell co-culture. A detailed description of the related methods is provided in the Supplementary Information.

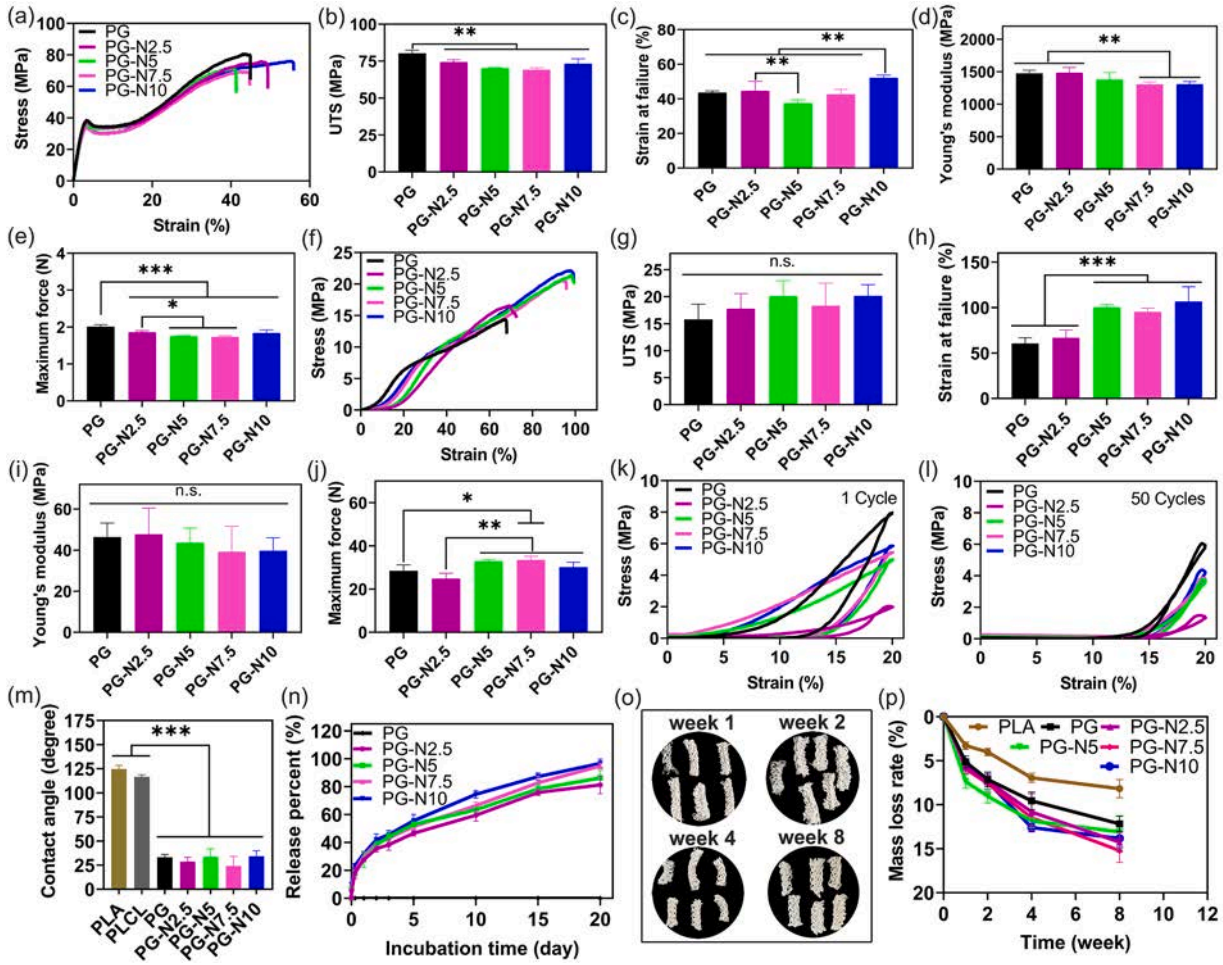

Fig. 3. Representative tensile stress-strain curves (a), UTS (b), strain at failure (c), Young's modulus (d), and maximum force (e) of DY. Representative tensile stress-strain curves (f), UTS (g), strain at failure (h), Young's modulus (i), maximum force (j), stress-strain curves for 1 cycle (k), stress-strain curves for 50 cycles (l) of knitting scaffolds. The water contact angle of PLA micron yarn, PLCL, and knitting scaffolds (m). The cumulative release percent of NPS in knitting scaffolds was quantified by an ultraviolet spectrophotometer (n). The images of freeze-dried knitting scaffolds after degradation (o), and the knitting scaffolds were: PLA micron yarn, PG, PG-N2.5, PG-N5, PG-N7.5, PG-N10 in order from left to right and from top to bottom. The mass loss rate after knitting scaffolds degradation (p). n.s.: no significance, * $p < 0.05$, ** $p < 0.01$, *** $p < 0.001$. ($n = 3$).

2.5. *In vivo* biocompatibility and repair effects

The animal experiments have been approved by the Ethics Committee of Zhongke Testing Technology Services (Guangzhou) Co., Ltd.

To verify the biocompatibility of NPS *in vivo*, the nanofiber membrane on the surface of the knitting scaffold was buried under the skin of SD rats for a subcutaneous embedding test: SD rats were anesthetized by inhaling isoflurane and then shaved off their waist hair. A 1.5 cm incision was made in the middle of the waist to separate the skin and expose the subcutaneous muscles. The nanofiber membrane (10 mm × 10 mm) was embedded under the skin and then sutured. Penicillin was injected intramuscularly with 1×10^4 units once daily for 3 days ($n = 3$).

To verify the repair effect of the knitting scaffold *in vivo*, it was used for patellar tendon defects in rabbits: 3 % pentobarbital sodium (1 mL/kg) was injected into the auricular vein for anesthesia. A 3 cm long incision was made on the medial side of the knee joint to expose the patellar tendon. A full-thickness defect (2.5 mm × 20 mm) was made in the center of the patellar tendon. The knitting scaffold (2.5 mm × 20 mm) was sutured to the edge of the defective patellar tendon using a simple intermittent suture method. The skin was finally sutured together layer by layer. Penicillin was injected intramuscularly with 4×10^5 units once daily for 3 days ($n = 3$).

The repaired patellar tendon samples after 1, 3, and 5 months were fixed in 10 % formalin for 48 h, and dehydrated in a graded series of ethanol. Subsequently, the samples were embedded and sectioned, and the sections were treated with hematoxylin-eosin staining (H&E staining), Masson's trichrome staining (MT staining), immunofluorescence staining (CD86, CD68), and picrosirius red staining (PSR staining).

2.6. Statistical analysis

All data were expressed as mean ± standard deviation (SD) from three independent experiments with a minimum of three replicates for each condition. One-way analysis of variance (ANOVA) followed by Tukey's post hoc test was used to determine the statistical significance unless specified otherwise. The significant difference was considered at *p <0.05 and **$p < 0.01$, *** $p < 0.001$.

3. Results

3.1. Characteristics of DY and knitting scaffolds

The diameter of a single DY was 168 ± 16 μm, and the diameter of the nanofibers on the DY surface was 410 ± 93 nm (Fig. 2a & Fig. S1). The DY was composed of PLA micron yarn and surface-wrapped nanofiber membrane, and a single PLA micron yarn was composed of 12

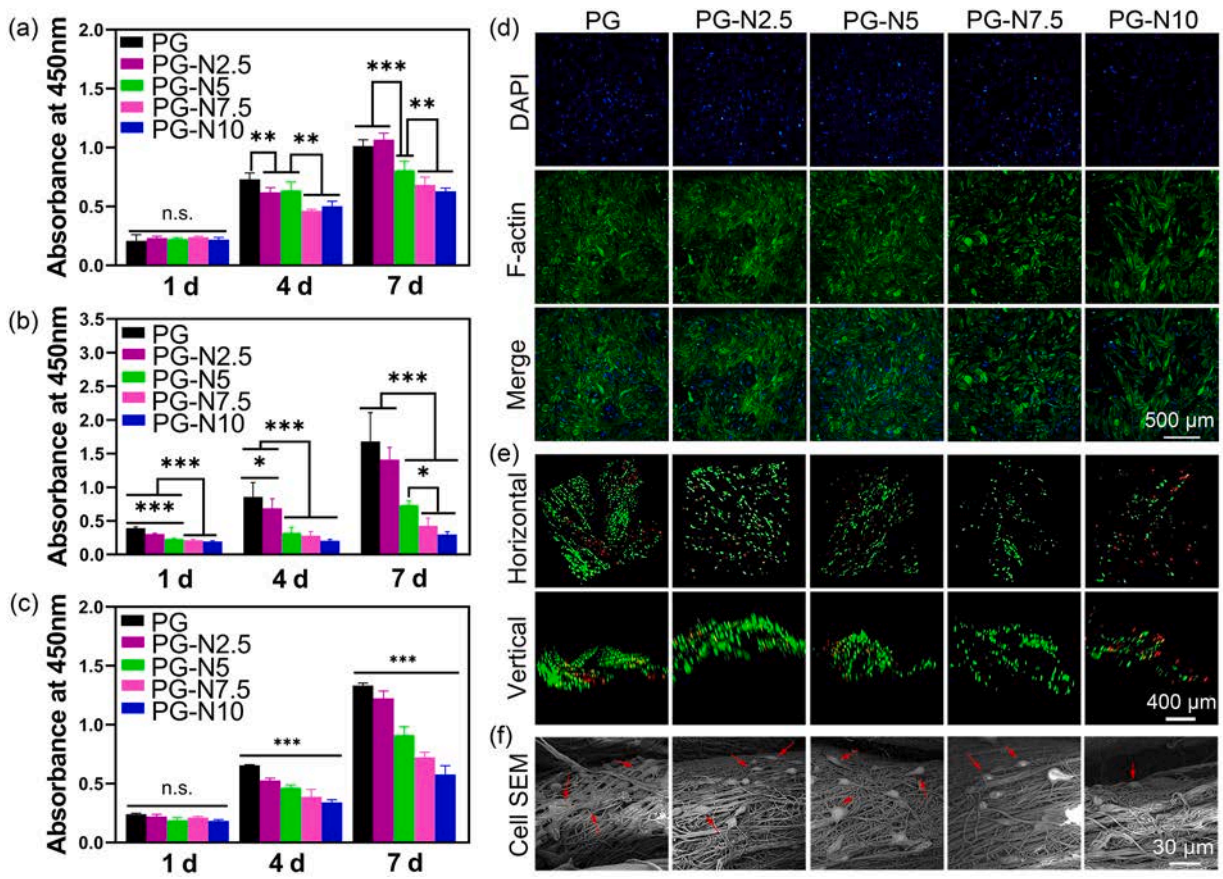

Fig. 4. The cytocompatibility of tenocytes, RAW264.7, and NIH 3T3. The proliferation of tenocytes (a), RAW264.7 (b), and NIH 3T3 (c) cultured on knitting scaffolds was measured using the CCK-8 assay. DAPI (blue) / F-actin (green) staining of tenocytes cultured in extraction solution after 10 days was observed using the inverted fluorescence microscope (d), scale bar = 500 μm. Live (green) / dead (red) staining for NIH 3T3 cultured on knitting scaffolds after 7 days was observed on the horizontal axis and vertical axis using the confocal microscope (e), scale bar = 400 μm. The cell morphology of NIH 3T3 cultured on knitting scaffolds after 7 days was observed under SEM (red arrows) (f), scale bar = 30 μm. n.s.: no significance, * $p < 0.05$, ** $p < 0.01$, *** $p < 0.001$. ($n = 3$). (For interpretation of the references to color in this figure legend, the reader is referred to the web version of this article.)

single filaments (Fig. 2b). The diameter of PLA micron yarn was 124 ± 34 μm, and the thickness of the double nanofiber membrane was 22 ± 6 μm (Fig. 2b). It could be seen that the diameter of the knitting scaffolds was 2.63 ± 0.2 mm (Fig. 2d).

The EDS results showed the presence of C, O, and Na elements in NPS-incorporated DY groups. However, no Na elements were detected in the PG group, while the content of Na elements increased with the increase of NPS in DY (Fig. 2c). The FTIR results showed that the ester group of 1755 cm^{-1} absorption peak proved the existence of PLCL, and the amide bond of 1643 cm^{-1} absorption peak proved the existence of Gel (Fig. 2e). EDS and FTIR results demonstrated that NPS, PLCL and Gel had been successfully spun into nanofibers. The TGA results showed that the main decomposition temperature of the knitting scaffolds was between 250 °C and 400 °C. The mass loss was more than 80 % at 400 °C, which was mainly related to the decomposition of the PLA micron yarn. Therefore, the knitting scaffolds exhibited good thermal stability (Fig. 2f).

The DY initially appeared a linear elastic region, and the plastic deformation exceeded the yield point with the increase of strain (Fig. 3a). The average value of ultimate tensile strength (UTS) was 73.5 ± 4.37 MPa (Fig. 3b). The average value of strain at failure was 44.11 ± 5.51 % (Fig. 3c). The average value of Young's modulus was 1390.04 ± 100.83 MPa (Fig. 3d). The average value of maximum force was 1.84 ± 0.11 N (Fig. 3e). When the stress-strain curve showed a fracture point, the DY yarn was a complete fracture. The difference was that the knitting scaffold was cracked rather than completely fractured. Some mechanical properties of the knitting scaffold were not as good as the DY (Fig. 3f–i). However, the average value of the maximum force of the knitting scaffold was 29.98 ± 3.50 N, which was significantly higher than the maximum force of DY (1.84 ± 0.11 N) (Fig. 3j). The knitting scaffolds were stretched for 50 cycles under 20 % strain conditions, and the average stress loss of the knitting scaffolds was 29.11 ± 2.86 %, which met the requirements of subsequent tests (Fig. 3k & l).

The contact angles were 124.73 ± 3.85°, 116.62 ± 2.23°, 33.11 ± 3.05°, 28.62 ± 4.55°, 33.74 ± 8.21°, 24.11 ± 10.09° and 34.18 ± 5.88° for PLA micron yarn, PLCL, PG, PG-N2.5, PG-N5, PG-N7.5, and PG-N10 (Fig. 3m). PLA micron yarn and PLCL were hydrophobic materials, and the hydrophilic effect of the knitting scaffolds became better after adding Gel (Fig. 3m & Fig. S2). The knitting scaffold with more NPS was released slightly faster than those with less NPS, and the NPS could be released continuously for more than 20 days (Fig. 3n). The degradation results showed that the knitting scaffolds had complete shape and did not decompose after 1, 2, 4, and 8 weeks (Fig. 3o). Due to the addition of Gel, the knitting scaffolds degraded faster than PLA micron yarn. The average mass loss of the knitting scaffolds was 13.71 ± 1.5 %, and the PLA yarn was 8.18 ± 1.02 % (Fig. 3p).

3.2. *In vitro cytocompatibility*

The cell viability was bounded by 75 % to verify the cytotoxicity of NPS. The rBMSCs cytotoxicity results showed that PG-N2.5, PG-N5, and PG-N7.5 were not cytotoxic, and PG-N2.5 and PG-N5 could promote rBMSCs growth compared to PG (Fig. S3). The results showed that the cytotoxicity of RAW264.7 for PG-N2.5 and PG-N5 was not cytotoxic

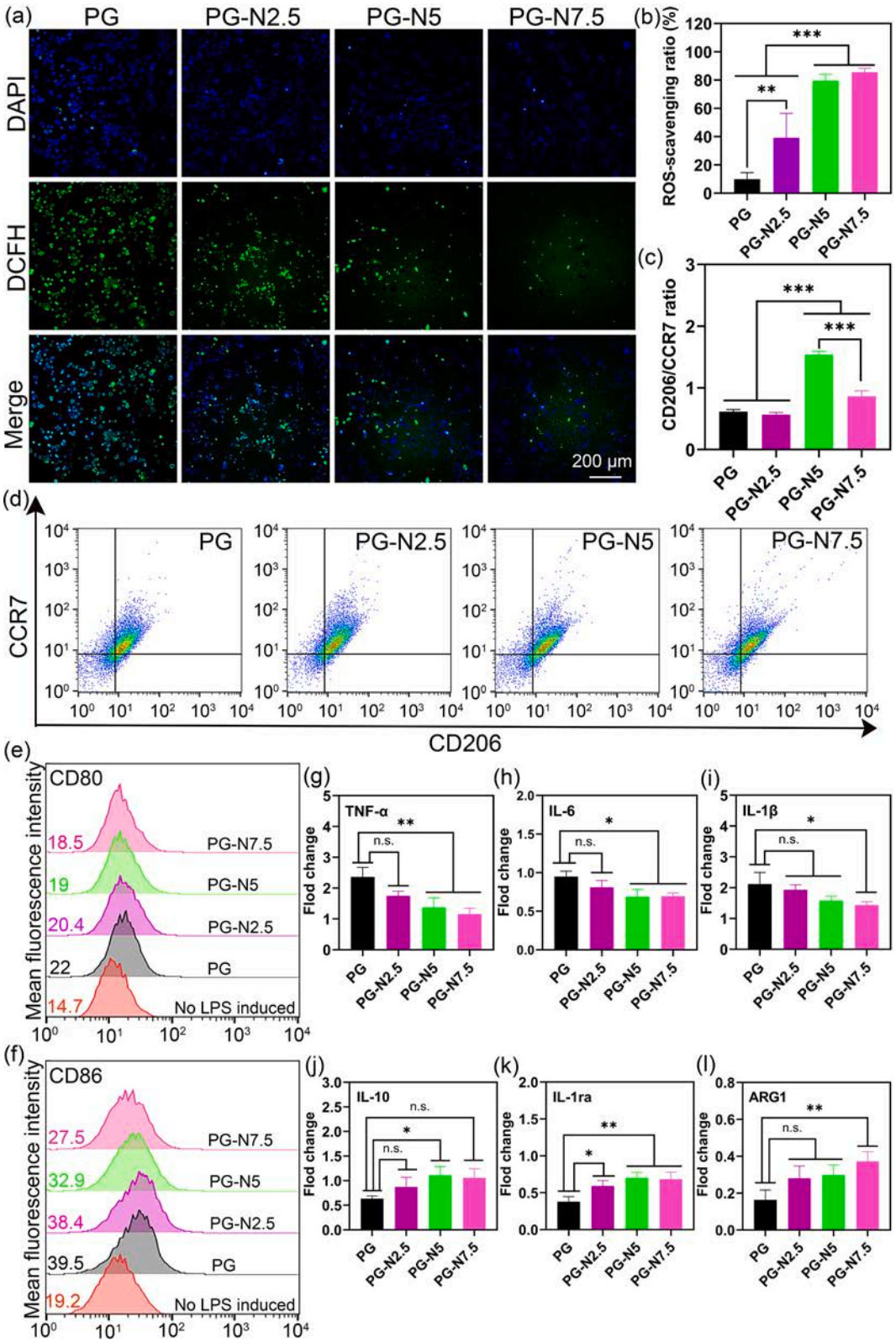

Fig. 5. The anti-oxidant ability of NPS: DAPI (blue) / DCFH-DA (green) staining of LPS-induced RAW264.7 cultured in extraction solution was observed using the inverted fluorescence microscope (a), scale bar = 200 μm. ROS-scavenging ratio (b). The anti-inflammatory ability of NPS: The macrophage markers CD206/CCR7 (c, d), CD80 (e), and CD86 (f) were analyzed by flow cytometer. The inflammatory cytokines TNF-α (g), IL-6 (h), IL-1β (i), IL-10 (j), IL-1ra (k), and ARG1 (l) were analyzed by Quantitative Real-time PCR (qPCR). n.s.: no significance, * $p < 0.05$, ** $p < 0.01$, *** $p < 0.001$. ($n = 3$).

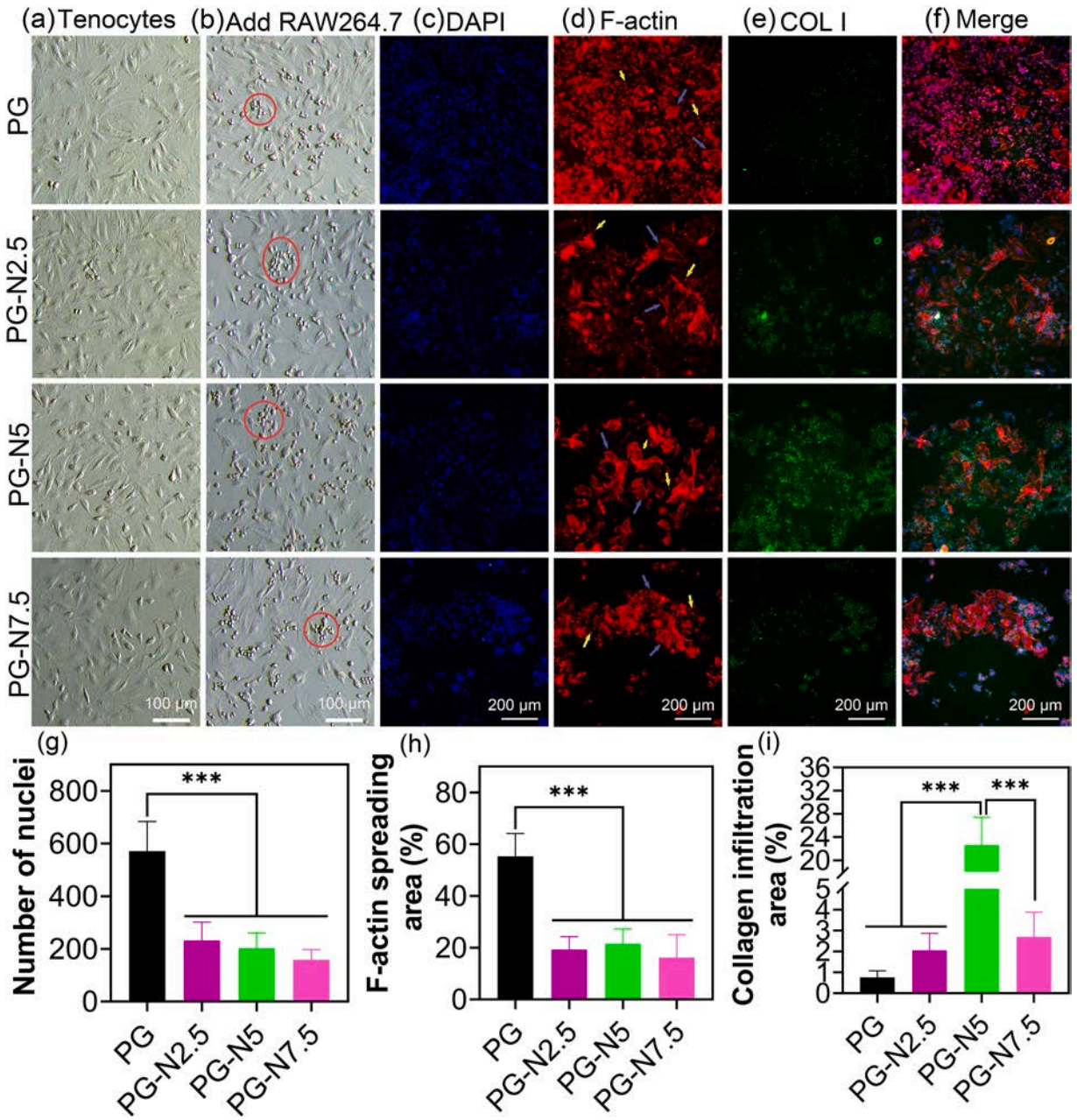

Fig. 6. The ability of tenocytes and RAW264.7 co-culture to express COL I. The primitive state of tenocytes (a), and the state of tenocytes and LPS-induced RAW264.7 co-culture (b), scale bar = 100 μm. DAPI (blue) / F-actin (red) / COL I (green) staining of tenocytes and LPS-induced RAW264.7 cultured in extraction solution was observed using the inverted fluorescence microscope (c, d, e) and merge figure (f), purple arrows: tenocytes, yellow arrows: RAW264.7, scale bar = 200 μm. Quantitative analysis of nuclei (g), F-actin spreading area (h), and collagen infiltration area (i) by using ImageJ software. *** $p < 0.001$. ($n = 3$). (For interpretation of the references to color in this figure legend, the reader is referred to the web version of this article.).

(Fig. S4).

The CCK-8 assay was used to evaluate cell proliferation behavior. The tenocytes showed a proliferative state on the knitting scaffold after 1, 4, and 7 days (Fig. 4a). The tenocytes spread well after 7 days, and the PG, PG-N2.5 and PG-N5 groups could completely spread with good cell morphology after 10 days (Fig. S5 & Fig. 4d). The RAW264.7 proliferation showed that the PG-N5, PG-N7.5, and PG-N10 groups were significantly lower than that of PG and PG-N2.5 after 4 and 7 days (Fig. 4b). The NIH 3T3 proliferation showed significant differences between all groups after 4 and 7 days (Fig. 4c). Then the live/dead fluorescence staining of NIH 3T3 on the knitting scaffold after 7 days were consistent with the results of CCK-8. It could be seen that NIH 3T3 could grow horizontally and vertically along the knitting scaffolds. However, the number of NIH 3T3 significantly decreased with the NPS increase (Fig. 4e). The SEM showed NIH 3T3 could extend on the surface of the knitting scaffolds (Fig. 4f). These proved that the knitting scaffolds could inhibit the excessive proliferation of foreign fibroblasts.

3.3. Anti-oxidant and anti-inflammatory effects of NPS

ROS released from RAW264.7 induced by LPS oxidized DCFH to produce green fluorescence. The number of positive RAW264.7 gradually decreased with increasing NPS concentration. This indicated that NPS could reduce the level of ROS in the upstream pathway of COX-2 (Fig. 5a & b).

To verify the inhibitory effect of NPS on inflammation in the

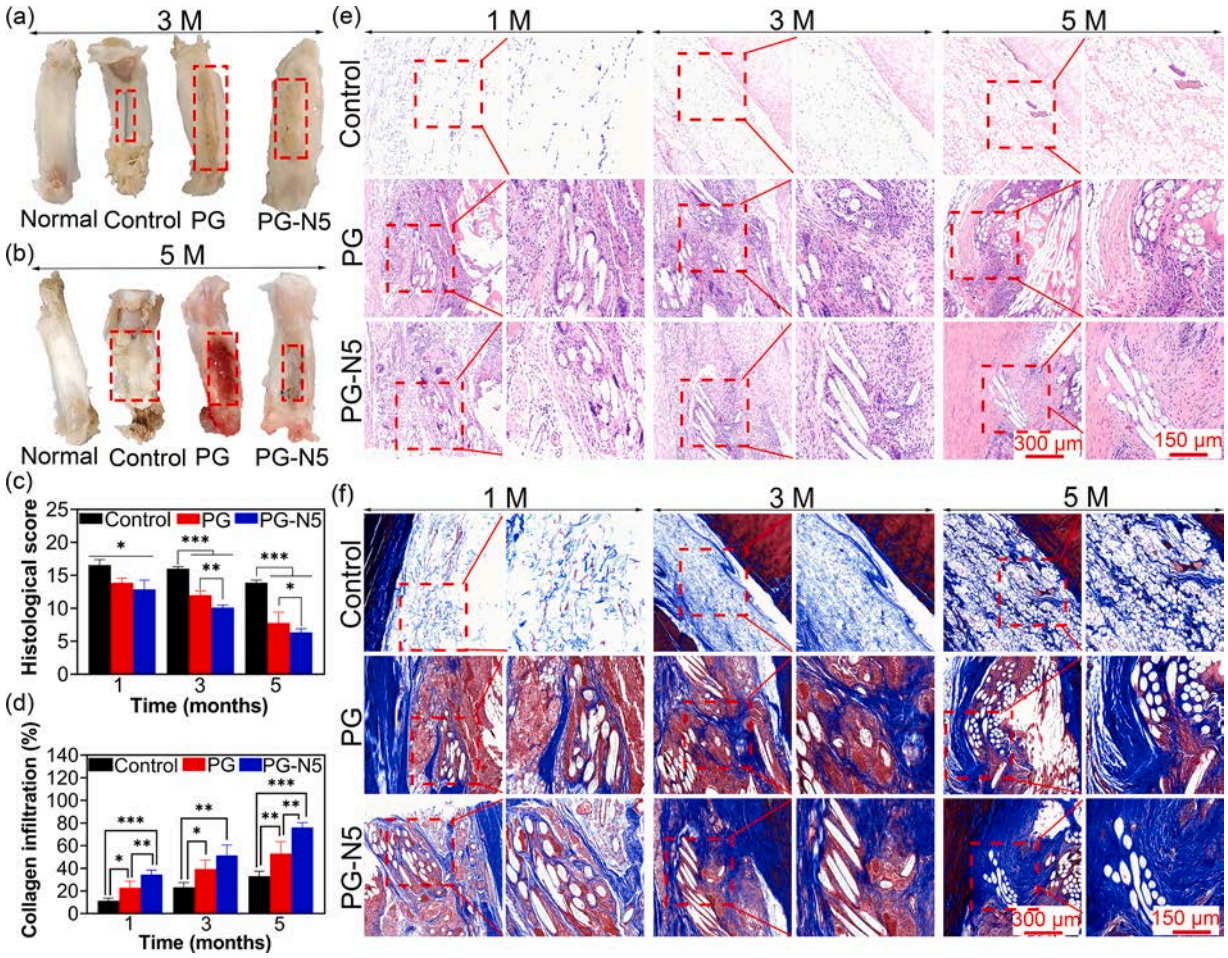

Fig. 7. Tendon reconstruction evaluation. Macroscopic view of knitting scaffold in tendon repair (a,b), histological score (c), collagen infiltration (d), H&E staining (e), MT staining (f). scale bar = 300 μm, and scale bar = 150 μm. Normal: native tendon. Control: defective untreated tendons. * $p < 0.05$, ** $p < 0.01$, *** $p < 0.001$. ($n = 3$).

downstream pathway, the expression of some common macrophage markers was analyzed by flow cytometry. Based on the ratio of CD206/CCR7 in the PG group being less than 1, LPS successfully induced M0 type RAW264.7 to M1 type (Fig. 5c & d). The CD206/CCR7 ratio increased in the PG-N5 and PG-N7.5 groups, indicating that RAW264.7 was converted to the M2 type in the presence of NPS. The anti-inflammatory effect was best in the PG-N5 group, while the lower value in the PG-N7.5 group of high NPS content was related to the toxicity of RAW264.7 (Fig. 5c & d). The mean fluorescence intensity values of CD80 and CD86 showed that the control group without LPS induction was lower than the PG and NPS-incorporated groups after LPS induction. The PG and NPS-incorporated groups were significantly shifted to the right compared to the control group, which better indicated that LPS-induced RAW264.7 was successfully shaped into the M1 type (Fig. 5e & f). It could be seen that the mean values of CD80 and CD86 decreased with increasing NPS content, in which the CD80 fluorescence intensity moved to the left slightly, while the CD86 fluorescence intensity moved to the left significantly. It indicated that NPS had a significant down-regulation effect on CD86 (Fig. 5e & f).

The effects of NPS on TNF-α, IL-6, IL-1β, IL-10, IL-1ra and ARG1 secreted by RAW264.7 were analyzed by qPCR. For the three pro-inflammatory cytokines, it was found that PG-N5 and PG-N7.5 could down-regulate TNF-α and IL-6, and PG-N7.5 also could down-regulated IL-1β (Fig. 5g–i). For the three anti-inflammatory cytokines, the PG-N5 significantly could up-regulate IL-10, and the NPS-incorporated groups all could up-regulate IL-1ra, while only PG-N7.5 could up-regulate ARG1 (Fig. 5j–l). From the results of qPCR, it could be seen that different NPS-incorporated groups had different effects for different cytokines. In other words, the anti-inflammatory effect did not necessarily increase with the increase of NPS levels, and there needed to be a moderate concentration to maintain balance in the organism.

3.4. RAW264.7 and tenocytes co-culture

Tenocytes were spread out in a spindle shape (Fig. 6a). RAW264.7 was added into tenocytes, and it showed a dotted distribution. However, when the LPS was added and induced RAW264.7 for 24 h, it was found that RAW264.7 preferred to bunch up and grow around the tenocytes (Fig. 6b & Fig. S6). With the addition of NPS, RAW264.7 in NPS-incorporated groups was transformed into M2 compared to the PG group, and the speed of RAW264.7 proliferation slowed down (Fig. 6c & d, g & h). It could be seen that the PG group was the majority of smaller-size M1 type RAW264.7 and few larger-size tenocytes co-existing. In contrast, the NPS-incorporated groups consisted of larger-size tenocytes and M2 type RAW264.7 surrounding the tenocytes. In other words, the dominant position gradually changed from M1 type RAW264.7 to tenocytes (Fig. 6d & f). Some studies have shown that macrophages in a polarized state can produce cytokines that affect fibroblasts, which promote collagen deposition and ECM remodeling [36]. In this test, it was demonstrated that the concentration of the NPS in PG-N5 is a suitable ratio, allowing the polarized macrophages to affect the tenocytes, and the tenocytes also act on macrophages. The two complement each other so that both cells enhance collagen expression (Fig. 6e & f). However, as previously demonstrated in tests, the PG-N7.5 group due to

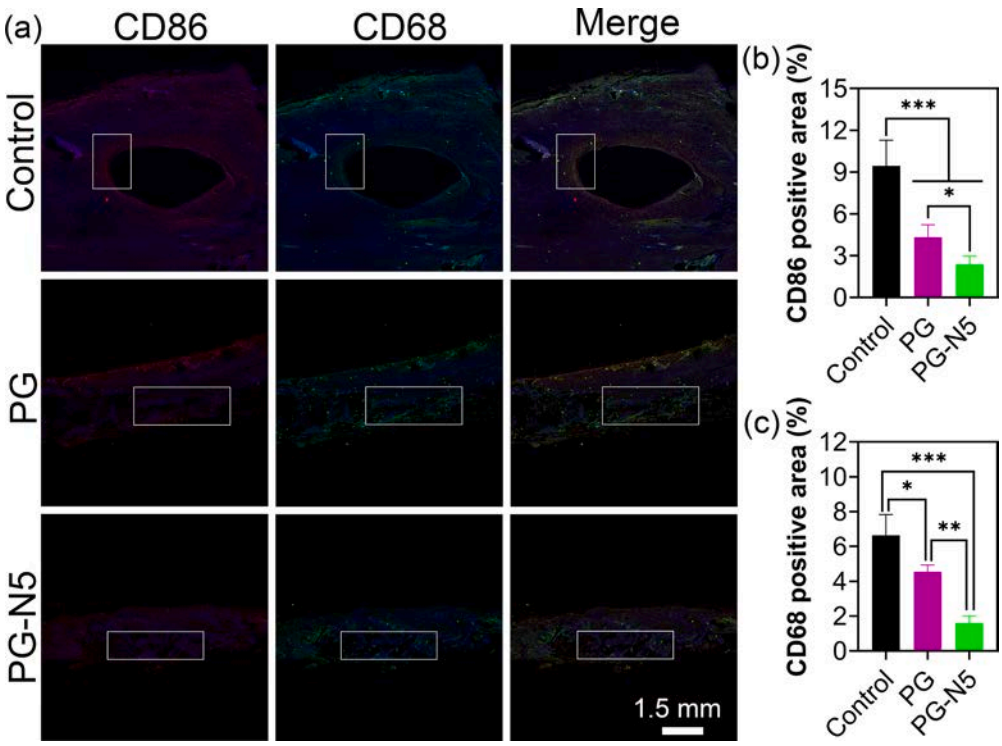

Fig. 8. Immunofluorescence staining of CD86 (red) and CD68 (green) expression at 1 month, and the nuclei were stained with DAPI (blue) (a), scale bar = 1.5 mm. Quantitative analysis of CD86 and CD68 expression positive areas by using ImageJ software (b, c). Control: defective untreated tendons. * $p < 0.05$, ** $p < 0.01$, *** $p < 0.001$. ($n = 3$). (For interpretation of the references to color in this figure legend, the reader is referred to the web version of this article.).

cytotoxicity had a lower ability to secrete COL I than PG-N5 (Fig. 6i). This demonstrated that PG-N5 was better suited to accelerate the transformation of macrophages and cause both cells to secrete more COL I.

In summary, the above cell test analysis showed that the PG-N5 group was non-toxic to rBMSCs and RAW264.7. It could inhibit the excessive proliferation of NIH 3T3. It had anti-oxidant, anti-inflammatory, and accelerated macrophage transformation effects. Therefore, the PG-N5 group was selected for patellar tendon defect repair in rabbits.

3.5. Tendon reconstruction evaluation

The subcutaneous embedding of SD rats showed that the PG-N5 group could reduce the inflammatory response and produce more collagen after 3 weeks, indicating that NPS had biocompatibility *in vivo* (Fig. S7). A defect model of the rabbit's patellar tendon was used to verify the repair ability of the PG and PG-N5 knitting scaffold, in which the control group was the defect without treatment. After 3 months, the control group showed significant defects compared to normal tendons. The knitting scaffolds in the PG and PG-N5 groups were surrounded by tissue, in which the PG-N5 knitting scaffold was surrounded by more tissue (Fig. 7a). After 5 months, the defect appeared hyperplasia in the control group. The exposed area of the knitting scaffold in the PG group decreased compared to the third month, but the repair effect was not very good. The PG-N5 knitting scaffold was almost covered by transparent glossy tendon-like tissue, which was similar to normal tendons (Fig. 7b).

The H&E staining showed that the defect in the control group had little cellular coverage and tissue regeneration was difficult (Fig. 7e). In both the PG and PG-N5 groups, the knitting scaffolds were infiltrated with cells and had tissue ingrowth. The inflammation decreased at each period as time increased, but the degree of inflammation was heavier in the PG group than in the PG-N5 group at all three time periods. The PG-N5 group showed almost no inflammation and had tendon-like tissue ingrowth after 5 months, indicating that NPS played an important role in balancing inflammation and laid the foundation for tendon recovery (Fig. 7c & e).

From MT staining, it could be seen that the regeneration rate of the control group was slow (Fig. 7f). After 5 months, the PG-N5 group found more collagen deposition in the space of the knitting scaffold compared to the PG group, which suggested that tendon tissue could gradually grow into the knitting scaffold of the PG-N5 group and replace it (Fig. 7d & f).

The immunofluorescence results after 1 month were consistent with HE staining. No cellular infiltration was seen in the defect area of the control group, however, CD86 and CD68 were highly expressed around the defect area. Compared with the control and PG groups, the PG-N5 group significantly down-regulated the expression levels of CD86 and CD68 (Fig. 8a–c). It indicated that the PG-N5 knitting scaffold had significant anti-inflammatory ability.

The ability of the control group to produce COL I was poor as seen from PSR staining (Fig. 9b). In the PG and PG-N5 groups, a small amount of collagen was observed on the surface of the knitting scaffolds after 1 month, and collagen fibers tended to grow into the knitting scaffolds (Fig. 9b). 3 months later, immature collagen was seen between the knitting scaffolds in the PG group, most of which were type III Collagen (COL III). At the same time, the mature COL I was required for tendon repair and could be seen between the knitting scaffolds in the PG-N5 group (Fig. 9b). After 5 months, a small amount of mature COL I was visible in the PG group. It's worth noting that a large amount of mature COL I could be seen surrounding the knitting scaffolds and partially covering them in the PG-N5 group. It suggested that the PG-N5 group was more favorable for the generation of COL I (Fig. 9a & b). The repaired tendon was stretched on a tensile machine, and when the machine displayed a sharp drop in the stress-strain curve, it could be seen that there was partial tissue tearing of the repaired tendon (Fig. 9c & d). The results showed that the recovery of mechanical properties in the PG-N5 group was better than that in the PG and control groups. Although

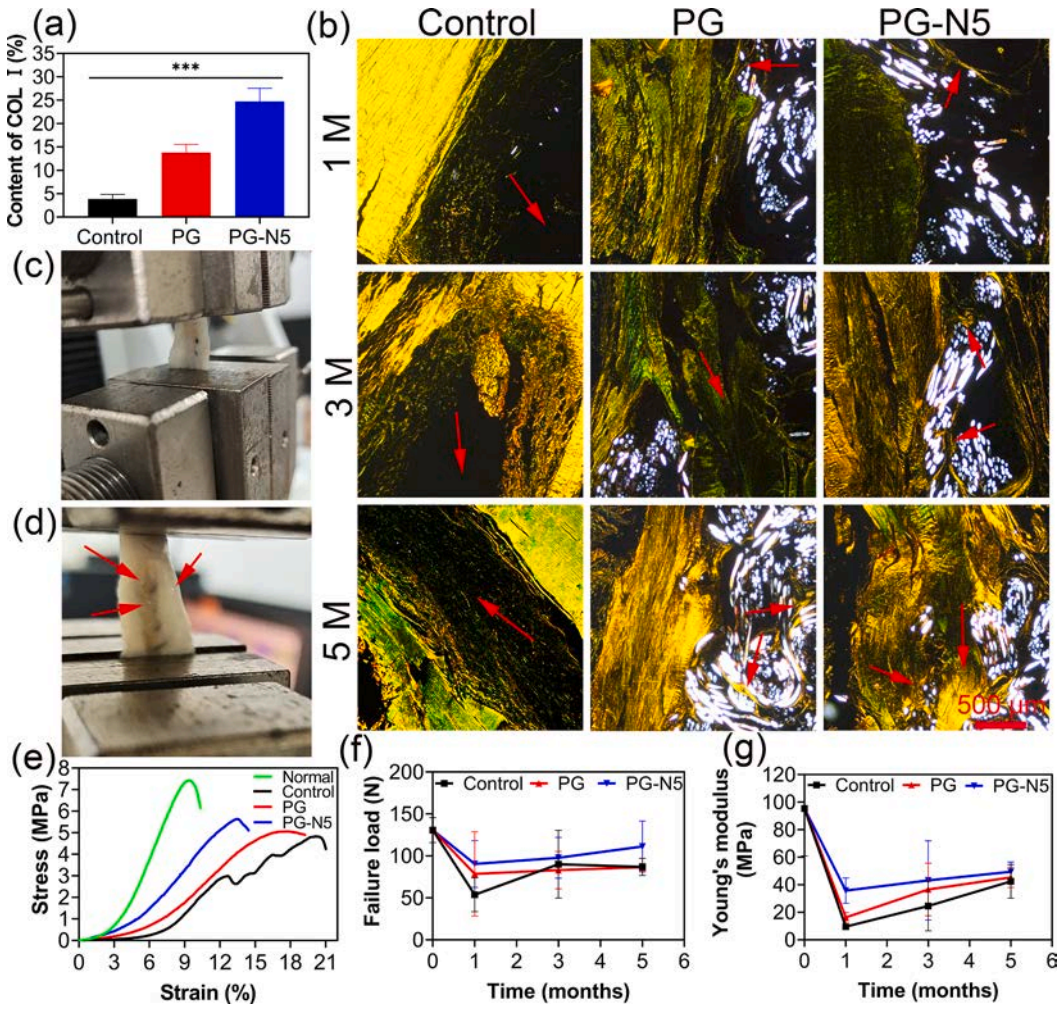

Fig. 9. The content of COL I after 5 months (a), PSR staining images (b), scale bar = 500 μm. The image before tendon strain (c), after tendon strain (d), and the stress-strain curve after 5 months (e). The change of failure load after 1, 3, and 5 months (f), the starting point of the failure load curve was obtained from the native tendon. The change of Young's modulus after 1, 3, and 5 months (g), the starting point of Young's modulus curve was obtained from the native tendon. Normal: native tendon. Control: defective untreated tendons. *** $p < 0.001$. ($n = 3$).

the mechanical properties of the PG-N5 group had not yet reached the level of normal tendons, the tendons of the PG-N5 group were in a stable recovery state (Fig. 9e–g).

4. Discussion

At present, nanofiber membranes obtained by electrospinning can be used to regulate inflammatory responses. Wang [37] et al. prepared the modified lubricated PLA nanofiber membrane that could significantly reduce the expressions of COL III and TNF-α. However, the mechanical properties of most anti-inflammatory nanofiber membranes are poor. Therefore, a scaffold that can satisfy both anti-inflammatory and good mechanical properties is very important in tendon repair. In this study, the alternative scaffolds were obtained for tendon repair by combining electrospinning and knitting technology (Fig. 1). The results of EDS and FTIR showed that the NPS-incorporated electrospinning knitting scaffold was prepared successfully (Fig. 2c & e). The knitting scaffold had better mechanical properties than single DY and nanofiber membranes, and it was more suitable for broken tendon repair with high mechanical (Fig. 3e & j). When the scaffold had been implanted *in vivo* for 5 months, as the tendon tissue tore during stretching, the scaffold in the tissue also tore at the same time. However, the scaffold did not break or detach from the tissue, and the two remained tightly bound together (Fig. 9c & d). To a certain extent, the scaffold matched the mechanical properties of the rabbit's tendon tissue.

Nowadays, more and more researchers are trying to avoid secondary surgeries by applying biodegradable materials instead of non-biodegradable materials to be implanted *in vivo* [38]. Degradable materials inevitably encounter mechanical deterioration during *in vivo* application. However, the reinforcement core of the knitting scaffold was made of PLA yarn, and the outer nanofibers contained PLCL, both of which were degradable but did not degrade too quickly, making them suitable for application in long-term procedures such as tendon repair (Fig. 3o). In a 5-month study in rabbits, it was found that the knitting scaffolds didn't loose *in vivo,* and the surface of the scaffold was encapsulated by tendon-like tissue (Fig. 7a & b). As the scaffold degraded, the tissue gradually grew in to replace the scaffold, eventually leading to tendon repair.

Macrophages play a key role in tendon repair. During the inflammatory state, macrophages accumulate in damaged tissue and coordinate various processes of tissue repair [39,40]. They usually change from the M1 type in the inflammatory phase to the M2 type in the proliferative phase. However, excessive accumulation of either type is detrimental. Excessive M1 leads to chronic inflammation and tissue destruction, and excessive M2 forms fibrosis [41]. Therefore, it is necessary to regulate macrophage transformation and balance the relationship between inflammatory response and tissue repair. In this study, NPS in the knitting scaffold could be released sustainably for

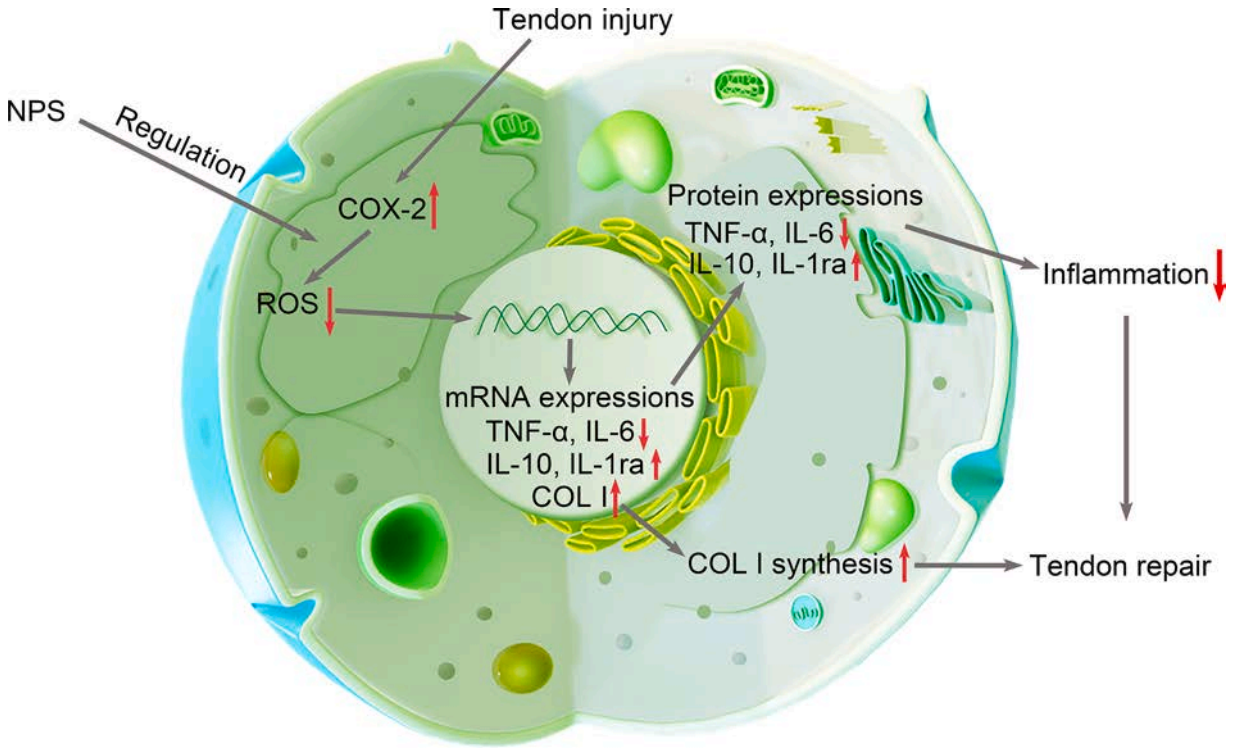

Fig. 10. Schematic diagram of the mechanism of NPS in tendon anti-inflammatory and pro-repair.

more than 20 days *in vitro*, which could meet the needs of balancing inflammation *in vivo* and lay the foundation for the later repair stage (Figs. 3n & 7e). NPS-incorporated knitting scaffold could slow down the proliferation of RAW264.7 (Fig. 4b). PG-N5 could reduce ROS level in the upstream pathway of COX-2 (Fig. 5a & b). PG-N5 had a significant down-regulation effect on CCR7 and CD86 (Fig. 5c & f). At the same time, PG-N5 also had a down-regulation effect on TNF-α and IL-6 in the downstream pathway of COX-2 (Fig. 5g & h). PG-N5 could also up-regulate the expression levels of IL-10 and IL-1ra secreted by RAW264.7 (Fig. 5j & k). These proved that the PG-N5 knitting scaffold had accelerated macrophage polarization and anti-inflammatory effects (Fig. 10).

Macrophages can regulate fibroblasts proliferation and ECM synthesis. Fibroblasts can regulate the polarization of macrophages by cytokine secretion or direct contact. Their interactions form a tight and delicate cycle during tendon repair [41,42]. Tenocytes are also a type of fibroblasts, tenocytes proliferation contributes to tendon repair. However, excessive proliferation of foreign fibroblasts can lead to tendon repair failure [43,44]. Therefore, it is necessary to inhibit the excessive proliferation of foreign fibroblasts and regulate the relationship between macrophages and tenocytes. In this study, the PG-N5 group could inhibit the excessive proliferation of NIH 3T3 (Fig. 4c). During the co-culture process, it was found that the PG-N5 group allowed RAW264.7 and tenocytes coexisted in a good state with a proper proportion. The two cells interacted to secrete more COL I, which made the PG-N5 knitting scaffold more suitable as an alternative scaffold for tendon repair (Fig. 6d & e). These proved that the PG-N5 knitting scaffold could regulate the relationship between macrophages and tenocytes and promote more COL I synthesis (Fig. 10).

Subcutaneous embedding in SD rats confirmed the good biocompatibility of NPS *in vivo* (Fig. S7). In the rabbit model of patellar tendon defect, the defect area in the control group showed tissue hyperplasia. Although the exposed area of the knitting scaffold was reduced in the PG group, the repair effect was still much worse compared to the normal tendon. It's worth noting that the PG-N5 group had no hyperplasia or inflammation, and transparent tendon-like tissue appeared, demonstrating the feasibility of NPS in anti-inflammatory (Fig. 7b). The knitting scaffold of the PG-N5 group played an important role in balancing inflammation and promoting collagen regeneration (Figs. 7c–f & 8). Among them, the PG-N5 group produced more COL I after 5 months (Fig. 9a & b). The mechanical properties of the PG-N5 group were improved and superior to the other two groups (Fig. 9e–g). These showed that the knitting scaffold of PG-N5 could play an important role in the anti-inflammatory and long-term repair of tendons.

The LARS artificial ligaments are mostly used in clinical [45,46]. It has high strength and little trauma, which can help patients recover movement early. However, the LARS artificial ligament is expensive and has complications such as enlarged bone tunnels and synovitis. The reason for this complication is the poor biological activity of PET, which makes it difficult for osseointegration in the bone tunnel. It's worth noting that the materials chosen for knitting scaffolds are biodegradable and have the advantage of being biocompatible, recruiting cells, and accelerating osseointegration[12,47]. At the same time, the NPS is added to the knitting scaffolds, which can reduce inflammation. In addition, this materials price of the knitting scaffold is low, which can reduce costs compared to the expensive LARS artificial ligaments. However, the mechanical properties of the knitting scaffold are not as good as LARS artificial ligaments, which is a common problem with degradable materials. At the same time, the healing process in rabbits is faster than in humans, and the knitting scaffolds had only been applied to a rabbit patellar tendon defect model. Therefore, the knitting scaffold and LARS artificial ligament need to be applied to various models of large animals for research in the future, and continuously optimize and improve the knitting scaffold during this process.

5. Conclusions

In this study, an anti-inflammatory 3D adjustable knitting scaffold with good mechanical properties was successfully prepared by combining electrospinning and knitting technology. The PG-N5 knitting scaffold could effectively inhibit the excessive proliferation of foreign

fibroblasts, regulate macrophage polarization, and promote tenocytes and RAW264.7 to generate more COL I. In the rabbit's patellar tendon defect model, the PG-N5 knitting scaffold could reduce inflammation, promote collagen regeneration, especially COL I, and effectively improve the mechanics of the repaired tendon. In a word, the knitting scaffold played a significant role in regulating inflammation and promoting tendon repair.

Declaration of competing interest

The authors declare that they have no known competing financial interests or personal relationships that could have appeared to influence the work reported in this paper.

Data availability

Data will be made available on request.

Acknowledgements

This research was supported by Science and Technology Commission of Shanghai Municipality, China (No. 20S31900900, 20DZ2254900) and Sino German Science Foundation Research Exchange Center, China (M-0263), China Education Association for International Exchange (2022181). This project was also supported by Researchers Supporting Project Number (RSP2024R65), King Saud University, Riyadh, Saudi Arabia. This project was also funding by Science and Technology Projects in Guangzhou (No. 202201020056) and the Clinical Frontier Technology Program of the First Affiliated Hospital of Jinan University, China (No. JNU1AF-CFTP-2022-a01204). This project was also supported by the Fundamental Research Funds for the Central Universities (CUSF-DH-T-2023063).

Supplementary materials

Supplementary material associated with this article can be found, in the online version, at doi:10.1016/j.apmt.2024.102070.

References

[1] L.J. Ning, Y.J. Zhang, Y.J. Zhang, M. Zhu, W. Ding, Y.L. Jiang, Y. Zhang, J.C. Luo, T.W. Qin, Enhancement of migration and tenogenic differentiation of macaca mulatta tendon-derived stem cells by decellularized tendon hydrogel, Front. Cell Dev. Biol. 9 (2021) 651583.
[2] Q. Zhang, Y. Yang, D. Suo, S. Zhao, J.C.-W. Cheung, P.H.-M. Leung, X. Zhao, A biomimetic adhesive and robust janus patch with anti-oxidative, anti-inflammatory, and anti-bacterial activities for tendon repair, ACS. Nano 17 (17) (2023) 16798–16816.
[3] J. Zhang, C. Xiao, X. Zhang, Y. Lin, H. Yang, Y.S. Zhang, J. Ding, An oxidative stress-responsive electrospun polyester membrane capable of releasing anti-bacterial and anti-inflammatory agents for postoperative anti-adhesion, J. Controll. Release 335 (2021) 359–368.
[4] K.T. Shalumon, C. Sheu, C.H. Chen, S.H. Chen, G. Jose, C.Y. Kuo, J.P. Chen, Multi-functional electrospun antibacterial core-shell nanofibrous membranes for prolonged prevention of post-surgical tendon adhesion and inflammation, Acta Biomater. 72 (2018) 121–136.
[5] R. Giancola, F. Oliva, M. Gallorini, N. Michetti, C. Gissi, F. Moussa, C. Antonetti Lamorgese Passeri, A. Colosimo, A.C. Berardi, CD200 as a potential new player in inflammation during rotator cuff tendon injury/repair: an in vitro model, Int. J. Mol. Sci. 23 (23) (2022) 15165.
[6] H. Shen, R.A. Lane, Extracellular vesicles from primed adipose-derived stem cells enhance achilles tendon repair by reducing inflammation and promoting intrinsic healing, Stem Cells 41 (6) (2023) 617–627.
[7] L. Dong, L. Li, Y. Song, Y. Fang, J. Liu, P. Chen, S. Wang, C. Wang, T. Xia, W. Liu, L. Yang, MSC-derived immunomodulatory extracellular matrix functionalized electrospun fibers for mitigating foreign-body reaction and tendon adhesion, Acta Biomater. 133 (2021) 280–296.
[8] C. Cai, X. Zhang, Y. Li, X. Liu, S. Wang, M. Lu, X. Yan, L. Deng, S. Liu, F. Wang, C. Fan, Self-healing hydrogel embodied with macrophage-regulation and responsive-gene-silencing properties for synergistic prevention of peritendinous adhesion, Adv. Mater. 34 (5) (2022) 2106564.
[9] J. Cai, J. Xu, Z. Ye, L. Wang, T. Zheng, T. Zhang, Y. Li, J. Jiang, J. Zhao, Exosomes derived from kartogenin-preconditioned mesenchymal stem cells promote cartilage formation and collagen maturation for enthesis regeneration in a rat model of chronic rotator cuff tear, Am. J. Sports Med. 51 (5) (2023) 1267–1276.
[10] X. Yu, J. Cui, Y. Shen, W. Guo, P. Cai, Y. Chen, Z. Yuan, M. Liu, M. El-Newehy, H. El-Hamshary, Y. Morsi, B. Sun, M. Shafiq, X. Mo, Current advancements and strategies of biomaterials for tendon repair: a review, Front. Biosci. 28 (4) (2023) 66.
[11] C. Akduman, I. Ozguney, E.P.A. Kumbasar, Preparation and characterization of naproxen-loaded electrospun thermoplastic polyurethane nanofibers as a drug delivery system, Mater. Sci. Eng. C 64 (2016) 383–390.
[12] Y. Chen, M. Shafiq, M. Liu, Y. Morsi, X. Mo, Advanced fabrication for electrospun three-dimensional nanofiber aerogels and scaffolds, Bioact. Mater. 5 (4) (2020) 963–979.
[13] Q. Zhang, Y. Yang, L. Yildirimer, T. Xu, X. Zhao, Advanced technology-driven therapeutic interventions for prevention of tendon adhesion: design, intrinsic and extrinsic factor considerations, Acta Biomater. 124 (2021) 15–32.
[14] M. Alimohammadi, Y. Aghli, O. Fakhraei, A. Moradi, M. Passandideh-Fard, M. H. Ebrahimzadeh, A. Khademhosseini, A. Tamayol, S.A. Mousavi Shaegh, Electrospun nanofibrous membranes for preventing tendon adhesion, ACS. Biomater. Sci. Eng. 6 (8) (2020) 4356–4376.
[15] C.T. Chen, C.H. Chen, C. Sheu, J.P. Chen, Ibuprofen-loaded hyaluronic acid nanofibrous membranes for prevention of postoperative tendon adhesion through reduction of inflammation, Int. J. Mol. Sci. 20 (2019) 5038.
[16] S. Jiang, X. Zhao, S. Chen, G. Pan, J. Song, N. He, F. Li, W. Cui, C. Fan, Down-regulating ERK1/2 and SMAD2/3 phosphorylation by physical barrier of celecoxib-loaded electrospun fibrous membranes prevents tendon adhesions, Biomaterials 35 (37) (2014) 9920–9929.
[17] A. Sensini, C. Gotti, J. Belcari, A. Zucchelli, M.L. Focarete, C. Gualandi, I. Todaro, A.P. Kao, G. Tozzi, L. Cristofolini, Morphologically bioinspired hierarchical nylon 6,6 electrospun assembly recreating the structure and performance of tendons and ligaments, Med. Eng. Phys. 71 (2019) 79–90.
[18] S. Wu, R. Zhou, F. Zhou, P.N. Streubel, S. Chen, B. Duan, Electrospun thymosin Beta-4 loaded PLGA/PLA nanofiber/microfiber hybrid yarns for tendon tissue engineering application, Mater. Sci. Eng. C 106 (2020) 110268.
[19] X. Xie, J. Xu, J. Lin, J. Jiang, Y. Huang, J. Lu, Y. Kang, Y. Hu, J. Cai, F. Wang, T. Zhu, J. Zhao, L. Wang, A regeneration process-matching scaffold with appropriate dynamic mechanical properties and spatial adaptability for ligament reconstruction, Bioact. Mater. 13 (2022) 82–95.
[20] J. Cai, X. Xie, D. Li, L. Wang, J. Jiang, X. Mo, J. Zhao, A novel knitted scaffold made of microfiber/nanofiber core-sheath yarns for tendon tissue engineering, Biomater. Sci. 8 (16) (2020) 4413–4425.
[21] X. Xie, J. Cai, Y. Yao, Y. Chen, A.u.R. Khan, J. Wu, X. Mo, A woven scaffold with continuous mineral gradients for tendon-to-bone tissue engineering, Composites Part B: Engineering 212 (2021) 108679.
[22] P. Li, H. Zhou, T. Tu, H. Lu, Dynamic exacerbation in inflammation and oxidative stress during the formation of peritendinous adhesion resulted from acute tendon injury, J. Orthop. Surg. Res. 16 (1) (2021) 293.
[23] Y. Li, L. Zou, T. Li, D. Lai, Y. Wu, S. Qin, Mogroside V inhibits LPS-induced COX-2 expression/ROS production and overexpression of HO-1 by blocking phosphorylation of AKT1 in RAW264.7 cells, Acta Biochim. Biophys. Sin. 51 (4) (2019) 365–374.
[24] Z. Yao, Y. Qian, Y. Jin, S. Wang, J. Li, W.E. Yuan, C. Fan, Biomimetic multilayer polycaprolactone/sodium alginate hydrogel scaffolds loaded with melatonin facilitate tendon regeneration, Carbohydr. Polym. 277 (2022) 118865.
[25] R. Nakano, T. Kitanaka, S. Namba, N. Kitanaka, Y. Suwabe, T. Konno, J. Yamazaki, T. Nakayama, H. Sugiya, Non-transcriptional and translational function of canonical NF-kappaB signaling in activating ERK1/2 in IL-1beta-induced COX-2 expression in synovial fibroblasts, Front. Immunol. 11 (2020) 579266.
[26] C. Yang, L. Nilsson, M.U. Cheema, Y. Wang, J. Frokiaer, S. Gao, J. Kjems, R. Norregaard, Chitosan/siRNA nanoparticles targeting cyclooxygenase type 2 attenuate unilateral ureteral obstruction-induced kidney injury in mice, Theranostics. 5 (2) (2015) 110–123.
[27] Z. Ju, M. Li, J. Xu, D.C. Howell, Z. Li, F.-E. Chen, Recent development on COX-2 inhibitors as promising anti-inflammatory agents: the past 10 years, Acta Pharm. Sin. B 12 (6) (2022) 2790–2807.
[28] M. Shafiq, Y. Chen, R. Hashim, C. He, X. Mo, X. Zhou, Reactive oxygen species-based biomaterials for regenerative medicine and tissue engineering applications, Front. Bioeng. Biotechnol. 9 (2021) 821288.
[29] K. Lu, M. Zhou, L. Wang, Y. Wang, H. Tang, G. He, H. Wang, C. Tang, J. He, W. Wang, K. Tang, Y. Wang, Z. Deng, N-Acetyl-ʟ-cysteine facilitates tendon repair and promotes the tenogenic differentiation of tendon stem/progenitor cells by enhancing the integrin α5/β1/PI3K/AKT signaling, BMC. Mol. Cell Biol. 24 (1) (2023) 1.
[30] A. Yurdasiper, G. Ertan, C.M. Heard, Enhanced delivery of naproxen to the viable epidermis from an activated poly N-isopropylacrylamide (PNIPAM) Nanogel: skin penetration, modulation of COX-2 expression and rat paw oedema, Nanomedicine 14 (7) (2018) 2051–2059.
[31] Y.S. Lui, M.P. Lewis, S.C. Loo, Sustained-release of naproxen sodium from electrospun-aligned PLLA-PCL scaffolds, J. Tissue Eng. Regen. Med. 11 (4) (2017) 1011–1021.
[32] F. Imani, R. Karimi-Soflou, I. Shabani, A. Karkhaneh, PLA electrospun nanofibers modified with polypyrrole-grafted gelatin as bioactive electroconductive scaffold, Polymer 218 (2021) 123487.
[33] X. Liu, C. Laurent, Q. Du, L. Targa, G. Cauchois, Y. Chen, X. Wang, N. de Isla, Mesenchymal stem cell interacted with PLCL braided scaffold coated with poly-ʟ-

lysine/hyaluronic acid for ligament tissue engineering, J. Biomed. Mater. Res. A 106 (12) (2018) 3042–3052.
[34] H. Samadian, A. Ehterami, A. Sarrafzadeh, H. Khastar, M. Nikbakht, A. Rezaei, L. Chegini, M. Salehi, Sophisticated polycaprolactone/gelatin nanofibrous nerve guided conduit containing platelet-rich plasma and citicoline for peripheral nerve regeneration: *in vitro* and *in vivo* study, Int. J. Biol. Macromol. 150 (2020) 380–388.
[35] X. Liu, X. He, D. Jin, S. Wu, H. Wang, M. Yin, A. Aldalbahi, M. El-Newehy, X. Mo, J. Wu, A biodegradable multifunctional nanofibrous membrane for periodontal tissue regeneration, Acta Biomater. 108 (2020) 207–222.
[36] F.C. Simoes, T.J. Cahill, A. Kenyon, D. Gavriouchkina, J.M. Vieira, X. Sun, D. Pezzolla, C. Ravaud, E. Masmanian, M. Weinberger, S. Mayes, M.E. Lemieux, D. N. Barnette, M. Gunadasa-Rohling, R.M. Williams, D.R. Greaves, L.A. Trinh, S. E. Fraser, S.L. Dallas, R.P. Choudhury, T. Sauka-Spengler, P.R. Riley, Macrophages directly contribute collagen to scar formation during zebrafish heart regeneration and mouse heart repair, Nat. Commun. 11 (1) (2020) 600.
[37] Y. Wang, Y. Xu, W. Zhai, Z. Zhang, Y. Liu, S. Cheng, H. Zhang, In-situ growth of robust superlubricated nano-skin on electrospun nanofibers for post-operative adhesion prevention, Nat. Commun. 13 (1) (2022) 5056.
[38] J. Cai, J. Wang, K. Ye, D. Li, C. Ai, D. Sheng, W. Jin, X. Liu, Y. Zhi, J. Jiang, J. Chen, X. Mo, S. Chen, Dual-layer aligned-random nanofibrous scaffolds for improving gradient microstructure of tendon-to-bone healing in a rabbit extra-articular model, Int. J. Nanomed. 13 (2018) 3481–3492.
[39] F. Wu, M. Nerlich, D. Docheva, Tendon injuries: basic science and new repair proposals, EFORT. Open. Rev. 2 (7) (2017) 332–342.
[40] N.L. Leong, J.L. Kator, T.L. Clemens, A. James, M. Enamoto-Iwamoto, J. Jiang, Tendon and ligament healing and current approaches to tendon and ligament regeneration, J. Orthop. Res. 38 (1) (2020) 7–12.
[41] J. Hou, R. Yang, I. Vuong, F. Li, J. Kong, H.Q. Mao, Biomaterials strategies to balance inflammation and tenogenesis for tendon repair, Acta Biomater. 130 (2021) 1–16.
[42] X. Zhou, R.A. Franklin, M. Adler, J.B. Jacox, W. Bailis, J.A. Shyer, R.A. Flavell, A. Mayo, U. Alon, R. Medzhitov, Circuit design features of a stable two-cell system, Cell 172 (4) (2018), 744–757 e17.
[43] M.Y. Hsiao, A.C. Lin, W.H. Liao, T.G. Wang, C.H. Hsu, W.S. Chen, F.H. Lin, Drug-loaded hyaluronic acid hydrogel as a sustained-release regimen with dual effects in early intervention of tendinopathy, Sci. Rep. 9 (1) (2019) 4784.
[44] T. Lei, T. Zhang, W. Ju, X. Chen, B.C. Heng, W. Shen, Z. Yin, Biomimetic strategies for tendon/ligament-to-bone interface regeneration, Bioact. Mater. 6 (8) (2021) 2491–2510.
[45] S. Li, S. Wang, W. Liu, C. Zhang, J. Song, Current strategies for enhancement of the bioactivity of artificial ligaments: a mini-review, J. Orthop. Translat. 36 (2022) 205–215.
[46] T. Chen, J. Jiang, S. Chen, Status and headway of the clinical application of artificial ligaments, Asia Pac. J. Sports Med. Arthrosc. Rehabil. Technol. 2 (1) (2015) 15–26.
[47] M. Silva, F.N. Ferreira, N.M. Alves, M.C. Paiva, Biodegradable polymer nanocomposites for ligament/tendon tissue engineering, J. Nanobiotechnol. 18 (1) (2020) 23.